Modeling the Thermal Effects of Artificial Turf on the Urban Environment

NEDA YAGHOOBIAN AND JAN KLEISSL

Mechanical and Aerospace Engineering, University of California, San Diego, La Jolla, California

E. SCOTT KRAYENHOFF

Department of Geography, The University of British Columbia, Vancouver, British Columbia, Canada

(Manuscript received 13 February 2009, in final form 22 September 2009)

ABSTRACT

The effects of artificial turf (AT) on the urban canopy layer energy balance, air and surface temperatures, and building cooling loads are compared to those of other common ground surface materials (asphalt, concrete, and grass) through heat transfer modeling of radiation, convection, and conduction. The authors apply the Temperatures of Urban Facets in 3D (TUF3D) model—modified to account for latent heat fluxes—to a clear summer day at a latitude of 33° over a typical coastal suburban area in Southern California. The low albedo of artificial turf relative to the other materials under investigation results in a reduction in shortwave radiation incident on nearby building walls and an approximately equal increase in longwave radiation. Consequently, building walls remain at a relatively cool temperature that is similar to those that are adjacent to irrigated grass surfaces. Using a simple offline convection model, replacing grass ground cover with artificial turf was found to add 2.3 kW h m^{-2} day^{-1} of heat to the atmosphere, which could result in urban air temperature increases of up to 4°C. Local effects of AT on building design cooling loads were estimated. The increased canopy air temperatures with AT increase heat conduction through the building envelope and ventilation in comparison with a building near irrigated grass. However, in this temperate climate these loads are small relative to the reduction in radiative cooling load through windows. Consequently, overall building design cooling loads near AT decrease by 15%–20%. In addition, the irrigation water conservation with AT causes an embodied energy savings of 10 W h m^{-2} day^{-1}. Locally, this study points to a win–win situation for AT use for urban landscaping as it results in water and energy conservation.

1. Introduction

The thermal environment of a city has a multifaceted effect on the health of its dwellers and ecological and economic consequences at several scales. Thermal comfort, heat wave mortality, ozone formation, and building energy consumption and resulting carbon dioxide emissions are all impacted to varying degrees by the canopy layer thermal environment and its distinct character relative to rural areas, a difference that is often loosely referred to as the urban heat island. In many cities around the world the effect of urbanization on local climate, especially on canopy layer air and surface temperatures, is significant (Oke 1982; Oke et al. 1991; Dhakal and Hanaki 2002; Giridharan et al. 2004). Furthermore, the modified surface energy balance in urban areas significantly modifies micro- and mesoscale flow fields (Bornstein 1987).

The genesis of a city's thermal environment is frequently complex in nature and depends on numerous factors including latitude, ambient meteorology, urban canopy geometry and material thermal properties, and the amount and distribution of vegetation and anthropogenic activity. All of the above factors except meteorology are significantly under our control, and in the present study we investigate the thermal effects of altering canopy floor materials. This is motivated by the limited availability of irrigation water to cool cities in arid climates.

Artificial turf (AT) has become increasingly popular as an irrigation-free and maintenance-free urban surface for athletic fields, parks, golf courses, and residential and commercial properties. While it is indisputable that AT conserves irrigation water, the thermal impact on the

Corresponding author address: Jan Kleissl, Mechanical and Aerospace Engineering, University of California, San Diego, 9500 Gilman Dr. 0411, La Jolla, CA 92093-0411.
E-mail: jkleissl@ucsd.edu

DOI: 10.1175/2009JAMC2198.1

© 2010 American Meteorological Society

Unauthenticated | Downloaded 03/26/25 07:04 AM UTC

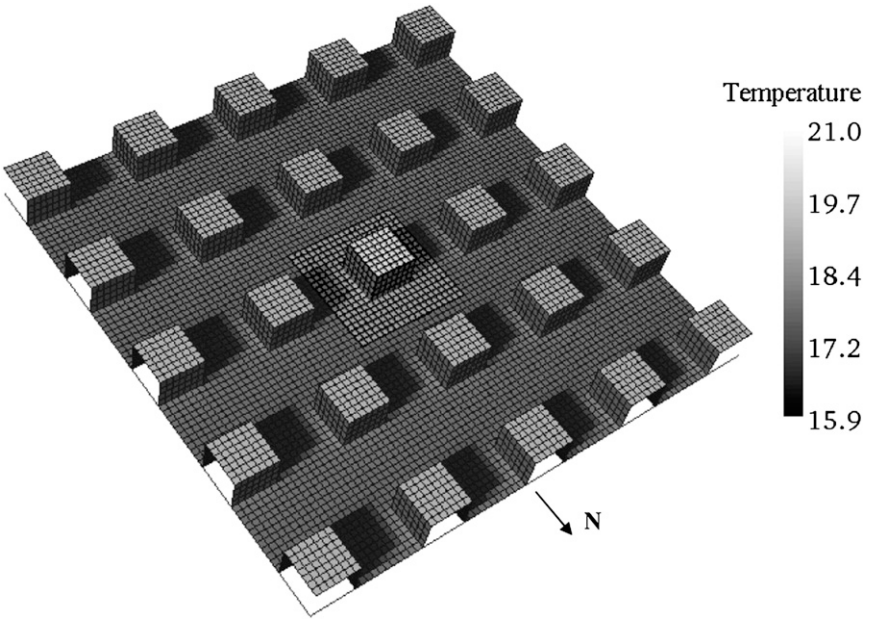

FIG. 1. TUF3D model simulation domain with buildings and ground showing surface temperature at 0700 LST. The length of each patch is equal to 3.75 m. The central urban unit is in lighter shades.

urban environment has not been quantified. Kruger and Pearlmutter (2008) showed that the cooling effect of open water evaporation on urban air temperature resulted in a 20%–80% reduction in building energy use in an arid area. However, these results cannot be generalized to grass surfaces (which are the major source of water vapor in urban areas through evapotranspiration) since grass has a larger solar reflectance (albedo) than most open water sources. The surface temperature of grass is usually close to the air temperature because of evaporative cooling. Anecdotal evidence suggests that the lack of evaporation allows AT surface temperatures to exceed those of regular grass by as much as 20°C (Galassi and Bortolin 2009). In this paper we apply a three-dimensional (3D) heat transfer model of the urban canopy to study the effects of AT on the energy balance of nearby buildings and the temperature of urban areas.

A description of the model is given in section 2, followed by results of the simulation in section 3. The sensitivity analysis in section 3e is followed by a discussion in section 4.

2. Methods

a. Modeling radiation, convection, and conduction with TUF3D

Temperatures of Urban Facets in 3D (TUF3D) is a microscale, three-dimensional, urban energy balance model designed to predict urban surface temperatures for a variety of surface geometries and properties, weather conditions, and solar angles (Krayenhoff and Voogt 2007, hereinafter KV07). The surface is composed of plane-parallel facets: roofs, walls, and ''streets.'' These facets are further subdivided into identical square patches, *each* of which has its own energy balance and surface temperature, resulting in a 3D raster model geometry (Fig. 1). TUF3D simulates the energy balance over such simple, nonvegetated, dry, 3D urban geometries on time scales from hours to days, resulting in surface temperature distributions down to the subfacet scale across walls, streets, and roofs. Its performance has been evaluated with several independent datasets (Krayenhoff 2005; KV07). A version of TUF3D optimized for geometries composed of repeating morphological units is used in this work.

A detailed description of TUF3D can be found in KV07 and only the main components are discussed here. TUF3D is structured into radiation, conduction, and convection submodels to determine sensible (Q_h), conduction (Q_g), and net radiative (R_{net}) fluxes (Fig. 2). The radiation submodel uses the radiosity approach (Ashdown 1994) and accounts for multiple reflections of direct solar radiation and shading. All radiative reflection and longwave emission is assumed perfectly diffuse, which enables radiative exchanges to be tracked with the use of view (or shape) factors.

In the conduction submodel of TUF3D a version of the one-dimensional (1D) heat conduction equation that

Unauthenticated | Downloaded 03/26/25 07:04 AM UTC

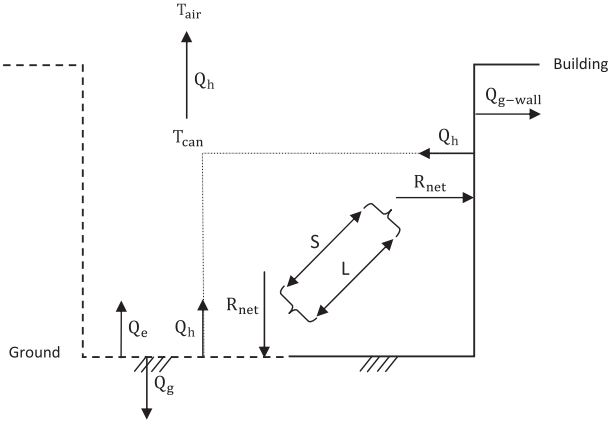

FIG. 2. Schematic of the energy balance components between building walls and ground surface in the urban canopy: T_{air}, above-canopy air temperature at twice the building height; T_{can}, canopy air temperature; R_{net}, net radiation; Q_h, sensible heat flux; Q_g, ground heat flux; $Q_{g\text{-wall}}$, building or wall heat flux; Q_e, latent heat flux; S, shortwave radiation; and L, longwave radiation. Note that in the model all calculations are conducted in three dimensions.

permits variable layer thickness and thermal conductivity is solved by finite differences for each patch (KV07).

Convection in TUF3D is modeled by relating patch heat transfer coefficients to the momentum forcing and the building morphology. Sensible heat flux from a patch i of any height follows the typical formulation:

$$H_i = h_i[T_{\text{sfc},i} - T_{\text{can}}(z_i)], \tag{1}$$

where h_i for *horizontal* patches is calculated using the stability coefficients of Mascart et al. (1995) and an effective wind speed, z_i is the height of the patch center plus a patch forcing height based on internal boundary layer arguments (Harman et al. 2004), and T refers to temperature. For *vertical* patches h_i in Eq. (1) is calculated based on a flat plate forced convection relationship using wind speed and temperature at the wall patch height, z_i (KV07). [In our simulations h_i averages approximately 21 W m^{-2} K^{-1} for the roof, 16 W m^{-2} K^{-1} for the walls, and for the ground surfaces varies from 9 W m^{-2} K^{-1} (concrete, asphalt) over 14 W m^{-2} K^{-1} (grass) to 17 W m^{-2} K^{-1} (AT).]

In the convection model the 1D wind speed profile is obtained by applying the logarithmic law above the canopy and an exponential profile within the canopy (KV07).

Advective horizontal exchanges are neglected in TUF3D because of the well-mixed nature of the canopy layer air in modeled domain, which is assumed to be embedded in a large area of similar land cover (here, a large suburban neighborhood).

The canopy air temperature T_{can} is calculated by means of an explicit energy budget of the volume of air inside the canopy (between buildings),

$$T_{\text{can}}^{m+1} = T_{\text{can}}^{m} + \frac{\Delta t(H_{\text{can}}^{m+1} - H_{\text{top}}^{m+1})}{c_{\text{air}}^{m+1}}, \tag{2}$$

where c_{air} (J m^{-2} K^{-1}) is the average heat capacity of air per unit plan area below the building height, H_{can} is the sum of the convective fluxes from all patches below the building height divided by the canopy–air–plan area ratio, H_{top} is the convective flux density of sensible heat across the canopy top (not including the roof), and m is the time index (KV07).

b. Modification to TUF3D

Our main focus is to compare the thermal effect of AT to grass (the surface that it would usually substitute) but we also present results for concrete and asphalt. Unlike AT, concrete, and asphalt, grass surfaces evaporate and transpire water, thereby cooling the surface and air. Consequently, TUF3D needs to be modified to account for the latent heat flux in the energy balance equation.

A realistic approach would involve a complex implementation of thermodynamic processes and fluid mechanics of water movement and phase transfer in the soil as well as aerodynamic, biologic, and energy balance principles to estimate both evaporation and transpiration (e.g., Grimmond and Oke 2002). In this study we are primarily concerned with the cooling properties of latent heat flux on the surface and air, but not in the urban water balance. Thus, we use the Bowen ratio ($\beta = Q_h/Q_e$) as an additional term in the energy balance equation to account for latent heat flux, Q_e, relative to the magnitude of sensible heat flux, Q_h. The general equation for energy balance at any patch surface (ground, walls, and roof) reads

$$(1-\alpha)K\downarrow^{m+1} + \epsilon[L\downarrow^{m+1} - \sigma(T_{\text{sfc}}^{m+1})^4] - \left(1+\frac{1}{\beta}\right)h^{m+1} \times [T_{\text{sfc}}^{m+1} - T^{m+1}(z)] - k_1(T_{\text{sfc}}^{m+1} - T_1^m)/\frac{1}{2}\Delta x_1 = 0, \tag{3}$$

where α is albedo, $K\downarrow$ and $L\downarrow$ are incident shortwave and longwave radiation, respectively (downwelling for ground and roof; horizontal for the walls), ϵ is the surface emissivity, σ is the Stefan–Boltzmann constant, and k_1 and Δx_1 are thermal conductivity and thickness of the first solid layer. We have omitted the i patch subscripts, and m refers to the time step. This equation is solved iteratively for T_{sfc}^{m+1} by Newton's method [similar to

Unauthenticated | Downloaded 03/26/25 07:04 AM UTC

Arnfield (1990)]. For nonvegetated areas the Bowen ratio term is excluded.

c. Geometry, initial, and boundary conditions

In the present study we use a 5×5 building array resolved by 79×79 patches in the horizontal resulting in a patch length of 3.75 m (Fig. 1). Buildings have square footprints of 26.25 m on a side and a height of $z_H = 15$ m. The distance between buildings is 41.25 m ($=2.75z_H$) in both x and y directions. Building plan area fraction (λ_p) is 0.15, the frontal area index is $\lambda_f = 0.086$, and the complete-to-plan area ratio (λ_c) is 1.35. This geometry is typical of a low-density North American suburban development without trees.

An ''urban unit'' defines the smallest plan area that encompasses all of the domain's morphological variation and repeats throughout the domain (KV07). Model outputs are computed over the urban unit in the center of the domain, while the remaining buildings provide appropriate radiative boundary conditions (Fig. 1).

The simulations start at 0000 LST and run for 24 h for a cloud-free day (yearday 172). While this is representative for summer days in California, our results do not apply for different meteorological conditions, especially cloudiness. However, by simulating the summer day with the largest insolation, we obtain an upper bound of the real effects of AT on urban temperatures and fluxes. Initial surface temperatures at 0000 LST are chosen to approximate thermal equilibrium. The initial air temperature inside the building is 22°C.

The top of the domain is in the atmospheric surface layer, where wind speed, above-canopy air temperature, and downwelling radiation are specified at twice the building height as follows: the model is forced with meteorological conditions for coastal Southern California (California climate zone 7), the largest market for artificial turf in the United States. The clear-sky downwelling shortwave radiation is calculated by the model for a latitude of 33°N. The wind speed is chosen to be constant at $U = 3$ m s^{-1}. The above-canopy air temperature T_{air} is set to the hourly average June air temperature from the Typical Meteorological Year (TMY3) at a representative coastal urban weather station (Miramar, call sign NKX, 32°52′N, 117°09′W, 146.9 m above mean sea level, and 10 km from the Pacific Ocean) in San Diego, California. Since it is impossible to simulate all possible scenarios, we present a sensitivity analysis in section 3e to determine representativeness and evaluate the potential for extrapolation of our results. This offline approach (i.e., using prescribed atmospheric forcing) ignores the feedback from the boundary layer, which serves to blunt the climatic response to surface modification. Hence, the simulations may be expected to provide an upper bound to the different energetic (and therefore climatic) responses to the different ground cover materials (Krayenhoff and Voogt 2004). The greater the influence of advection the less important local surface–atmosphere coupling becomes in terms of the evolution of boundary layer properties. Thus the offline approach is expected to overestimate the heating (negative) impacts of AT on the boundary layer, resulting in a more conservative estimate of its net benefit.

At the bottom of the domain, the temperature boundary condition at the base of the deepest substrate layer serves to drive conductive exchanges with a constant ''deep soil'' (ground) or ''internal'' (roofs and walls) temperature. The deep soil temperature is chosen as 16°C.

d. Material properties

1) Surface radiative and thermal properties

Table 1 presents thermal and radiative properties of AT, grass, asphalt, and concrete. Emissivities of these four materials are similar but their albedos differ significantly. Since no AT albedos could be found in the literature, the AT albedo was measured at two athletic fields with a Kipp and Zonen CM6 thermopile albedometer. Measurements at La Costa Canyon High School AT baseball field in Carlsbad, California, on 27 July 2008 from 1230 to 1300 PST as well as at the University of San Diego rugby field on 6 August 2008 at 1315–1345 PST both revealed an albedo of 0.08. The substrate of AT is polyethylene, and hence appropriate thermal properties were obtained (Table 1).

2) Subsurface thermal properties

For this idealized case study we chose typical thermal properties for each material and layer, but they will vary greatly in practice (Fig. 3). Following Jansson et al. (2006), for asphalt and concrete the top layer has a thickness of 0.07 m followed by 0.7 m of crushed rock and 0.6 m of clay soil with a volumetric soil water content of $\theta = 0.4$. We chose a base layer of AT as 5-mm polyethylene over 0.18 m of clay soil ($\theta = 0.1$) followed by 0.5 m of sandy soil ($\theta = 0.4$). Underneath the irrigated grass is a layer of loam soil ($\theta = 0.4$) of thickness 0.05 m over 0.08 m of clay soil with $\theta = 0.4$ followed by 0.1 m of clay soil with $\theta = 0.3$ and 0.5 m of sandy soil ($\theta = 0.4$). Note that the soil moisture is not dynamic or coupled to evapotranspiration, but merely affects heat conduction and storage in the subsurface. To improve the accuracy of the solution to the heat conduction equation in TUF3D, we subdivided these material layers into thinner computational layers and ensured that the

Unauthenticated | Downloaded 03/26/25 07:04 AM UTC

TABLE 1. Thermal and radiative properties of different ground materials.

	Grass	Artificial turf (polyethylene)	Asphalt	Concrete
Thermal conductivity (W m^{-1} K^{-1})	1.10[a]	0.42[b]	0.75[c]	1.51[c]
Heat capacity (J m^{-3} K^{-1})	$2.8^{a} \times 10^{6}$	$0.634^{b} \times 10^{6}$	$1.94^{c} \times 10^{6}$	$2.11^{c} \times 10^{6}$
Momentum roughness (m)	0.005[d]	0.005[d]	0.0005[e]	0.0005[e]
Thermal roughness (m)	0.0005[d]	0.0005[d]	0.0001[e]	0.0001[e]
Albedo (α) (–)	0.26[c]	0.08 (measurement)	0.18[f]	0.35[f]
Emissivity (ϵ) (–)	0.95[c]	0.95 (assumption)	0.95[c]	0.90[c]

[a] Campbell and Norman (1998).
[b] Speight (2005).
[c] Oke (1987).
[d] Brutsaert (1982).
[e] Chen et al. (1999).
[f] Iqbal (1983).

ratio of thicknesses between all adjacent layers was 3 or less. Since the thermal damping depths of the subsurface materials are less than 0.14 m, all materials below 0.14 m will not significantly affect our results.

3) BUILDING MATERIAL RADIATIVE AND THERMAL PROPERTIES

We assume an empty building with no anthropogenic heat production. Thermal and radiative properties of building walls and roof are presented in Table 2. The roof parameters are not critical to our study, since the roof does not interact with the ground surface materials. However, the wall parameters are important and their sensitivity will be analyzed in section 3e.

e. *Effects of ground surface properties on the urban canopy*

The different thermal and radiative properties of asphalt, concrete, grass, and AT (Table 1) result in different ground surface temperatures that in turn affect heat transfer to the urban canopy. If the choice of a ground surface material is motivated by building energy efficiency considerations, the thermal interactions between ground surfaces and buildings are of particular interest. Ground surface temperature affects building wall temperature (and heat flux) through longwave emission (L; Fig. 2); L is determined by surface temperature, emissivity, and view factors:

$$L_{\text{ground\_to\_wall}} = \psi_{\text{ground,wall}} \epsilon \sigma T^{4}_{\text{ground}}, \tag{4}$$

in which $L_{\text{ground\_to\_wall}}$ (W m^{-2}) is the upwelling longwave radiation, per unit area of ground, from ground patches incident on wall patches, $\psi_{\text{ground,wall}}$ is the wall view factor of the ground, and T_{ground} is the ground surface temperature, which depends on surface type.

Similarly, the transfer of heat from ground to wall through shortwave reflection is

$$S_{\text{ground\_to\_wall}} = \psi_{\text{ground,wall}} \alpha S_{\text{dn}}. \tag{5}$$

It depends on the ground surface albedo, α, view factor, and the incident global (direct and diffuse) shortwave flux density on the ground, S_{dn} (W m^{-2}). The net longwave and shortwave radiation between ground and wall are then calculated by substituting respective temperature, emissivity, albedo, and view factor in Eqs. (4) and (5):

$$\text{RL}_{\text{net}} = L_{\text{ground\_to\_wall}} - L_{\text{wall\_to\_ground}} \quad \text{and}$$
$$\text{RS}_{\text{net}} = S_{\text{ground\_to\_wall}} - S_{\text{wall\_to\_ground}}. \tag{6}$$

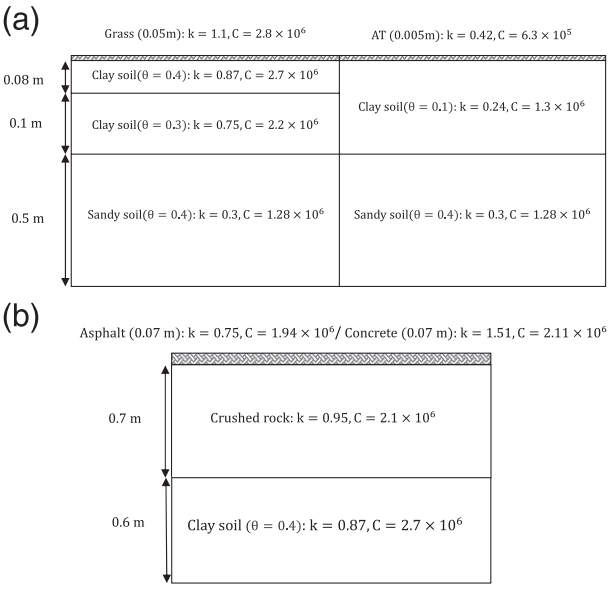

FIG. 3. (a) Subsurface layer depths and thermal properties for AT and grass surfaces; k is thermal conductivity (W m^{-1} k^{-1}), C is heat capacity (J m^{-3} K^{-1}), and θ is volumetric water content. (b) Subsurface layer depths and thermal properties for asphalt and concrete surfaces; k, C, and θ are defined as in (a).

Unauthenticated | Downloaded 03/26/25 07:04 AM UTC

TABLE 2. Thermal and radiative properties of building walls and roof.

	Wall			Roof			
	Plywood	R-13	Dry wall (gypsum)	Asphalt	Plywood	R-30	Dry wall (gypsum)
Thickness (m)	0.0127	0.088	0.0127	0.01	0.0127	0.2	0.0127
Thermal conductivity (W m^{-1} K^{-1})	0.12	0.038	0.17	0.75	0.12	0.038	0.17
Heat capacity (J m^{-3} K^{-1})	6.62×10^5	0.02×10^6	8.72×10^5	1.94×10^6	6.62×10^5	0.02×10^6	8.72×10^5
Albedo (α) (–)	0.3	—	—	0.15	—	—	—
Emissivity (ϵ) (–)	0.88	—	—	0.92	—	—	—

In the simple TUF3D convection model, ground surface temperature indirectly affects building wall temperatures through heating of the canopy air, which in turn modulates the wall–canopy air temperature difference and resulting wall heat flux [Fig. 2; Eq. (1)].

Heat fluxes and temperatures in the urban canopy vary over the course of the day. We will use maximum and aggregate quantities where appropriate to quantify the thermal impacts of the different ground surfaces on temperatures and heat fluxes on urban canopy temperatures and building energy use. *Maximum* surface and air temperatures and ground and wall energy balance fluxes are not directly related to total building energy use. However, they may be related to peak building energy use affecting electric grid stability and electricity rates. The *aggregate* heat fluxes (cumulative heat fluxes over a day; kW h m^{-2} day^{-1}) and their differences give better information on the total heat exchange and resulting building energy use.

f. Sensitivity study and limitations

In this first study of the thermal impact of AT, it is not possible to assess the full diversity of urban landscapes. Here we focus on an area and climate where AT is most common and most likely to see increased use. The low built-up fraction (15%) and the absence of roads may approximate suburban gated communities with narrow walkways, but these conditions are unrealistic for most residential areas. However, model limitations and a desire for generality motivate our simple approach. Since actual material properties and geometrical and meteorological conditions vary, we conducted a sensitivity analysis to determine the sensitivity of building wall T_{wall} and canopy air temperatures T_{can} to wind speed, above-canopy air temperature (T_{air}), ground properties (albedo, thermal conductivity, and heat capacity), geometric–radiative parameters (building plan area fraction, frontal area ratio, latitude), and Bowen ratio. We repeated the grass and AT simulations varying these parameters by ±20% and tabulated the resulting change in air and wall temperatures.

We acknowledge that the absence of field experimental data to validate our modeling results is a limitation of our study. However, conducting neighborhood scale field experimental studies of heat exchange is a cost- and labor-intensive task, and could not be afforded. Furthermore, TUF3D modeled surface temperatures have shown good agreement with observations from realistic urban environments (KV07).

3. Results

a. Diurnal cycle of urban temperatures

We choose grass as the reference surface, as it is still the most frequently used surface type in landscaping and community design. Figure 4 presents the temperatures of the urban facets, canopy air, and building internal air over 24 h. Results are averages over all patches that compose each surface or facet (e.g., ground, roofs, and walls). Temperature T_{wall} is the average temperature of all four walls of a building, each of which undergoes a very different diurnal cycle. The highest temperature of the urban surfaces on this day are 50.6°C for the roof (1200 LST), 31.3°C for ground (grass) (1300 LST), 31.6°C for building wall (1400 LST), and 23.6°C for canopy air (1200 LST). Because of evaporative cooling and reduced insolation, the ground temperature is lower than the roof temperature, but still larger than the canopy air temperature. The building wall surfaces remain cooler during midday since their vertical orientation causes them to receive less insolation. At night all of the urban surface temperatures are similar except for the roof where longwave cooling results in lower temperatures. Because of the insulating properties of the building materials, the internal building temperature has a small amplitude.

We now quantify the effects of other surface materials on the urban energy balance with a focus on artificial turf. Figure 5 compares ground, canopy air, and building wall temperatures for AT, asphalt, grass, and concrete surfaces over 24 h. While all urban surface temperatures are similar at night, all other materials become significantly warmer than grass during the day. The maximum ground temperature increases relative to grass by 21.2°C for asphalt (at 1300 LST), 22.6°C for AT (at

Unauthenticated | Downloaded 03/26/25 07:04 AM UTC

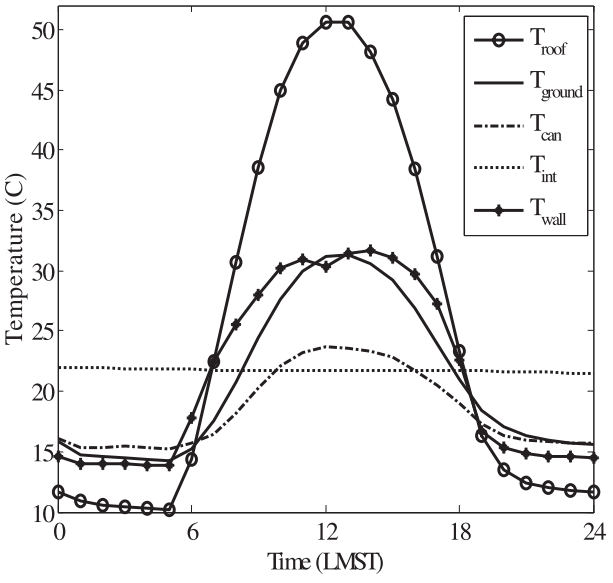

FIG. 4. Modeled urban facets, canopy air, and building internal air temperatures for a community covered with a grass surface on a clear summer day in coastal Southern California: T_{roof}, T_{ground}, T_{can}, T_{int}, and T_{wall} are the roof, ground, canopy air, internal building air, and building wall temperatures, respectively.

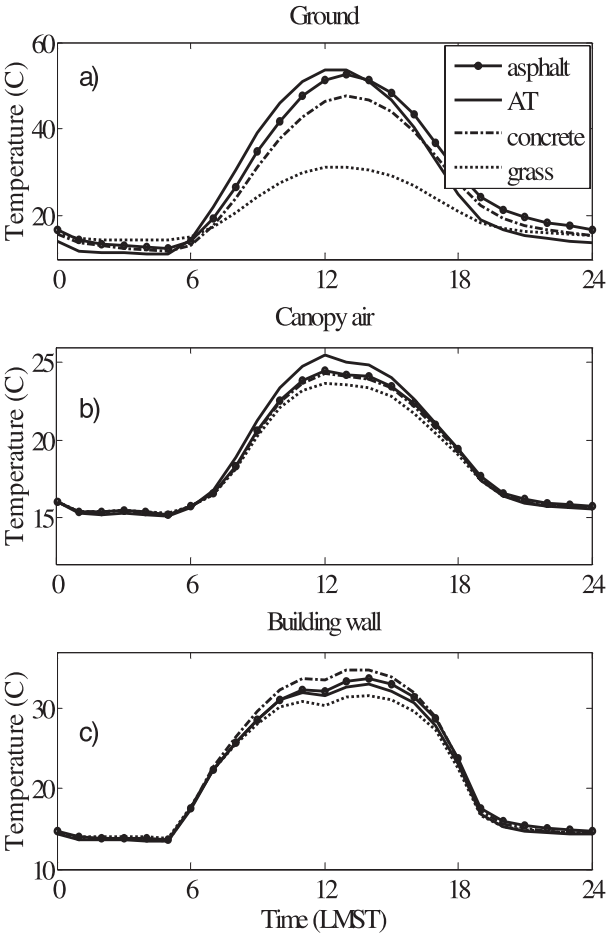

FIG. 5. Comparison of (a) ground surface, (b) canopy air, and (c) building wall average temperatures for AT, grass, asphalt, and concrete surfaces.

1200 LST), and 16.2°C for concrete (at 1300 LST). The peak ground temperatures for asphalt and concrete lag because of their larger thermal inertia. In contrast, the canopy air temperatures T_{can} all peak at 1200 LST and the maximum T_{can} for asphalt, AT, and concrete are 0.8°, 1.8°, and 0.6°C higher than for grass, respectively, assuming no coupling to boundary layer (forcing) temperature. Given almost constant interior building temperatures, building wall temperatures T_{wall} are linearly related to the conductive heat flux into the building. Peak average T_{wall} (at 1400 LST) for asphalt, AT, and concrete are 2.0°, 1.3°, and 3.1°C higher than that with grass ground cover, respectively. The difference between AT and grass is approximately constant between 1000 and 1400 LST, but it becomes negligible at about 1700 LST.

b. Diurnal cycle of urban heat fluxes

Figure 6 shows the energy balance components at the ground surface for grass and AT. Assuming $\beta = 0.3$, the latent heat flux Q_e is the dominant means of heat removal from the grass surface. For example, at noon Q_e is $0.57R_{\text{net}}$, Q_h is $0.17R_{\text{net}}$, and Q_g is $0.26R_{\text{net}}$. Over the day the total latent heat flux is 2.5 kW h m^{-2} implying an evaporation rate of 3.6 mm day^{-1} (per m^2 of grass) or 3.0 mm day^{-1} (per m^2 of urban area). Note that for the other ground materials (AT, asphalt, and concrete) $Q_e = 0$. The resulting increase in Q_h increases T_{can}.

Figure 7 shows energy balance components at the outside surface of the R-13 building wall for grass and AT ground covers. The maximum net radiation is about 140 W m^{-2} with a dip around noon when the small solar zenith angle reduces the shortwave radiation intensity per square meter of wall. Because of wall insulation the conductive flux into the building is much smaller than the convective flux. The wall net radiation for AT is slightly smaller than that for grass. However, the larger T_{can} leads to reduced temperature spread between canopy air and wall, and hence smaller Q_h.

c. Radiative exchange between building and ground

The direct impact of ground surface materials on urban energy use is primarily through radiative exchange between building and ground and resulting effects on T_{wall} and $Q_{g\text{-wall}}$ [Fig. 2; Eqs. (4)–(6)]. Since the emissivities of different materials are similar (Table 1), $L_{\text{ground\_to\_wall}}$ is strongly correlated with ground temperature to the

Unauthenticated | Downloaded 03/26/25 07:04 AM UTC

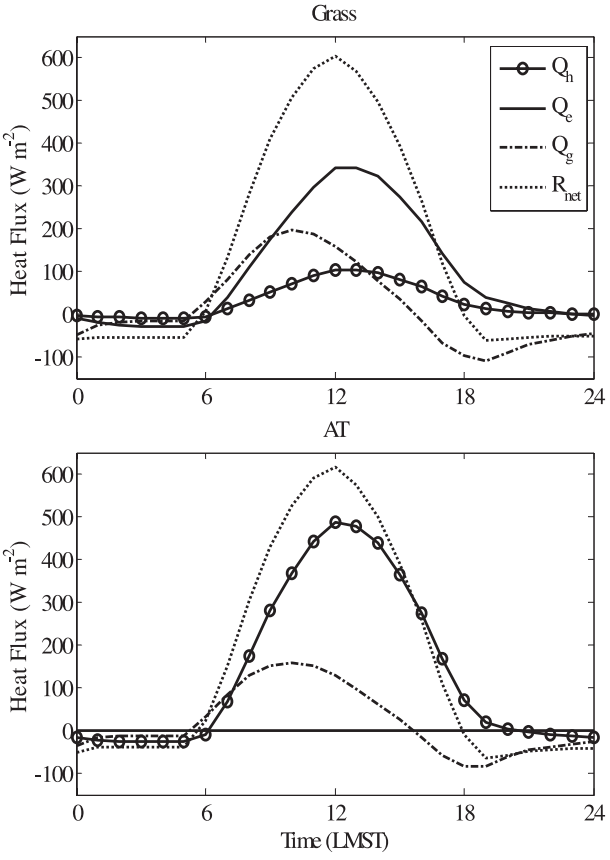

FIG. 6. Modeled energy balance components for the (top) grass and (bottom) AT surfaces; Q_h, Q_e, and Q_g are sensible, latent, and ground heat fluxes, respectively, and R_{net} is the net radiation.

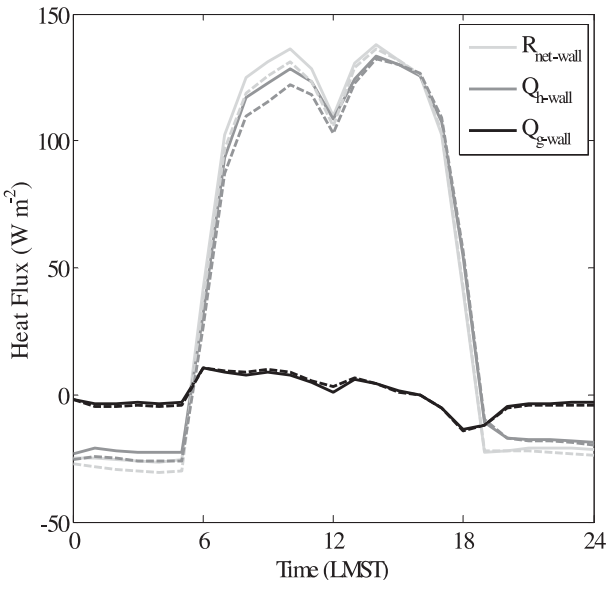

FIG. 7. Energy balance components averaged over the four walls for grass (solid line) and AT (dashed line); $Q_{h\text{-wall}}$ is the wall-to-canopy sensible heat flux, $Q_{g\text{-wall}}$ is the conduction heat flux into the wall, and $R_{\text{net-wall}}$ is the net radiation on the building walls after multiple reflections. Area units refer to wall surface area.

fourth power (Figs. 8a, 5a). Consequently, AT and asphalt transfer the most longwave radiative flux to the building, followed by concrete, and grass is a distant fourth. Ultimately, the radiative effect of a surface material is described by the net exchange of longwave radiation RL_{net} between building wall and ground. Since $L_{ground\_to\_wall}$ affects the wall temperature (Fig. 5c), there is a dynamic feedback on RL_{net} through $L_{wall\_to\_ground}$. The maximum RL_{net} (per unit area of wall surface) for AT is 39.7 W m^{-2} at 1200 LST, which is much larger than for grass (Table 3; Fig. 8d).

The impact of ground material properties on building wall temperature through shortwave radiation [Eqs. (5), (6)] is nontrivial, since multiple reflections of shortwave radiation occur in the urban canopy. In comparison with other surfaces, concrete shows the largest $S_{ground\_to\_wall}$ because of its higher albedo (0.35; Table 1), while AT shows the smallest $S_{ground\_to\_wall}$ (Fig. 8b). The maximum $S_{ground\_to\_wall}$ for AT is 34 W m^{-2} less than that for grass. Considering reflection of solar radiation from walls to the ground (wall albedo is 0.3), the maximum RS_{net} for AT is 8.41 W m^{-2} (per unit area of wall surface), which is significantly smaller than RS_{net} for other materials (Table 3; Fig. 8e). In fact, net shortwave radiation exchange with AT is a heat sink for building walls for most of the day.

The total upwelling radiative flux (the sum of longwave and shortwave radiative fluxes from the ground to the building wall) is similar for AT and grass, while asphalt and especially concrete show larger upwelling radiative fluxes (Fig. 8c). The net effect of different longwave and shortwave contributions is the overall net radiation between ground and building walls (Fig. 8f; in units of wall area). Relative to grass, the direct effect of AT is a reduction in net radiative heat flux between ground and building walls. The peak is reduced by 3.2 W m^{-2} and the 24-h total is reduced by 56 W h m^{-2} day^{-1}. This seems counterintuitive as AT surface temperatures are much larger than those for grass. However, the net radiation is dominated by the reduction in shortwave solar reflected radiation through the low albedo (Fig. 8e). Thus considering only radiative effects, installing AT cools adjacent buildings.

d. Convective heat exchange between building and ground

Ground materials indirectly affect building wall temperature, T_{wall}, through convection or Q_h, which is parameterized as a function of the temperature difference between surface and air [Eq. (1)]. Since above-canopy

Unauthenticated | Downloaded 03/26/25 07:04 AM UTC

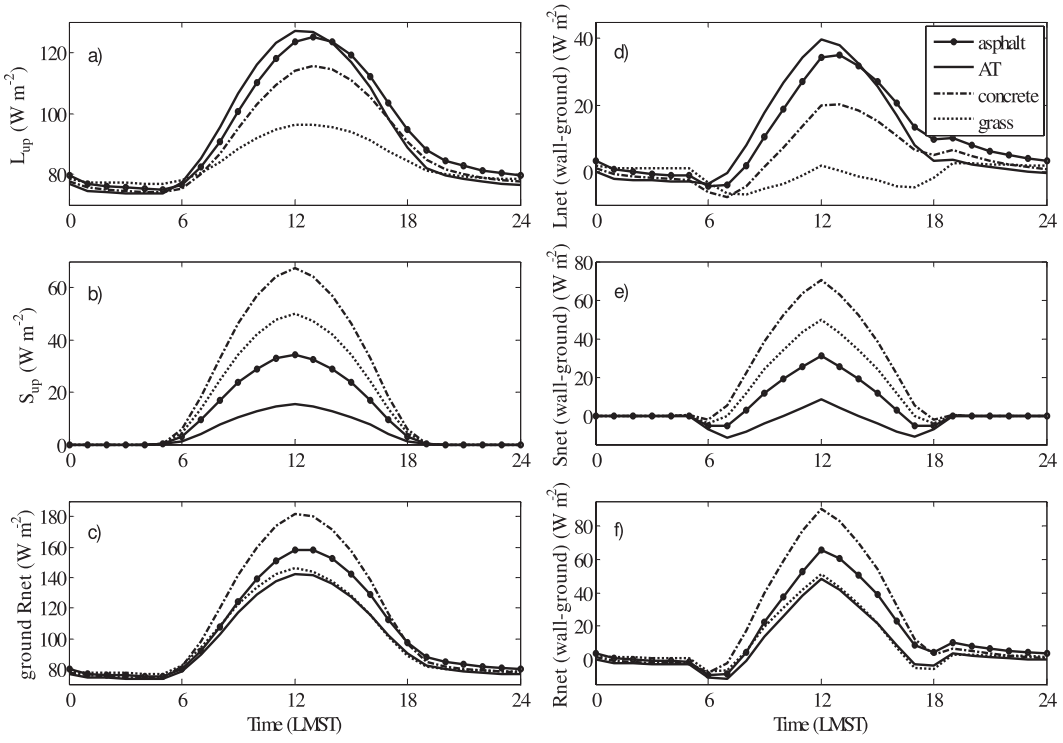

FIG. 8. (a) Longwave, (b) shortwave, and (c) total radiation from ground to building wall for different ground materials in watts per meter squared of ground surface area. (d) Net longwave radiation, (e) net shortwave radiation, and (f) net radiation flux between ground and building wall in watts per meter squared of wall.

air temperature is an input boundary condition in TUF3D, the indirect effect of urban ground materials on buildings is through increased T_{can} (Fig. 2). A larger ground-to-canopy Q_h increases T_{can}, which in turn reduces the building wall-to-canopy heat flux increasing T_{wall}.

As expected considering Eq. (1) and T_{can} in Fig. 5b, Fig. 9a shows that Q_h from the ground to the canopy air for AT is larger than for all other ground covers with a maximum of 487 W m^{-2} (Table 4). This compares to a maximum roof heat flux of 568 W m^{-2}.

The average Q_h from building walls to canopy air (Fig. 9b) increases throughout the day until wall temperatures reach their maximum around 1400 LST. Table 4 shows that the maximum convective heat transfer from wall to air with AT as ground cover is 132 W m^{-2}, which is less than for grass and significantly less than for concrete and asphalt.

Heat also escapes the urban canopy layer and is mixed throughout the atmospheric boundary layer (ABL), leading to nonlocal effects. Since the surface layer temperature T_{air} is prescribed as a fixed boundary condition (Fig. 2), the effect of different urban surfaces on temperatures in the urban surface layer and ABL cannot be obtained from TUF3D alone. To estimate these effects offline we assume that the sensible heat flux from the canopy heats the well-mixed, dry, and deep ABL equally over a depth of 2 km with 1.1 kg m^{-3} air density and

TABLE 3. Maximum radiative flux densities between ground and wall and their timing in the day. All maxima in shortwave radiation occur at 1200 LST.

	AT	Asphalt	Concrete	Grass
Max longwave (ground to wall) (W m^{-2} of ground)	127	125	115	96.4
Time (LST)	1200	1300	1300	1300
Max net longwave (W m^{-2} of wall)	39.7	34.9	20.3	1.8
Time (LST)	1200	1300	1300	1200
Max shortwave (ground to wall) (W m^{-2} of ground)	15.2	34.4	67.6	49.9
Max net shortwave (W m^{-2} of wall)	8.41	31.2	70.5	49.6

Unauthenticated | Downloaded 03/26/25 07:04 AM UTC

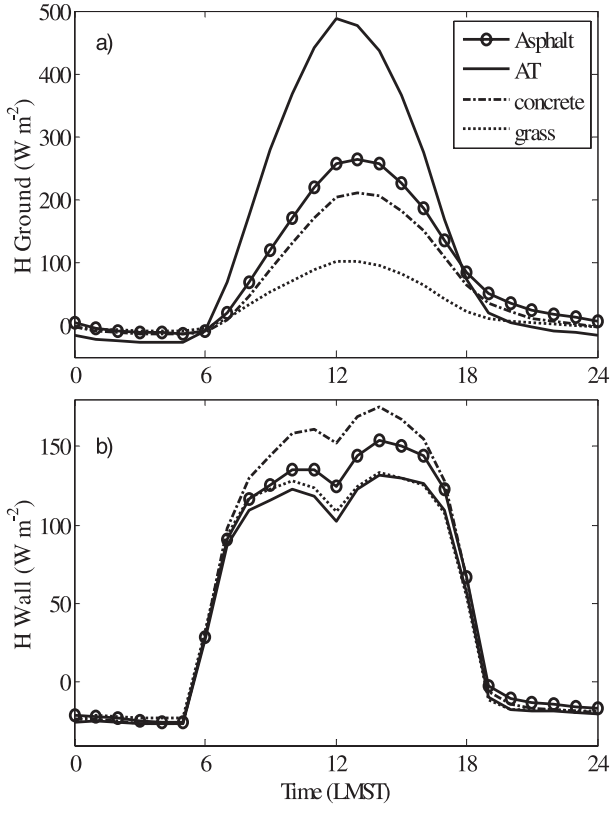

FIG. 9. Comparison of sensible heat flux from (a) ground and (b) building walls to canopy air for AT, grass, asphalt, and concrete. Building wall sensible heat fluxes are averaged over all walls and shown per unit of wall area.

1004.67 J kg^{-1} K^{-1} heat capacity. We do not consider the entrainment through the ABL top. In the first offline scenario the ABL air is assumed to linger or ''recirculate'' over the model domain and thus continues to accumulate the heat emitted by the surface. By accumulating the heat fluxes over a day we obtain the energy entering to the ABL and the resulting heating (Table 5). Relative to grass, AT emits an additional 2.3 kW h m^{-2} of heat to the ABL resulting in a temperature increase of 3.7°C. The offline nature of this scenario makes these numbers high estimates, as rising boundary layer temperatures resulting from increased sensible heat flux from the canopy air with AT would in reality blunt the process.

In the second more realistic offline scenario we consider the typical sea-breeze conditions in coastal areas with a shallower thermal internal boundary layer of 500-m thickness (Venkatram 2008). Assuming a mean boundary layer wind speed of 5 m s^{-1} we estimate the convective heating from the surface for each kilometer that it passes over an urban area. For this scenario, the temperature increases due to canopy sensible heat flux of grass, concrete, asphalt, and AT are 0.042°, 0.078°, 0.09°, and 0.15°C km^{-1}, respectively. The evaporation from grass increases the specific humidity by 2.86×10^{-4} g kg^{-1} km^{-1}.

e. Sensitivity study

Table 6 shows the sensitivity of the maximum wall and canopy air temperatures T_{can} to wind speed, ground properties, building geometry, Bowen ratio, above-canopy air temperature (T_{air}), and latitude for the grass and AT surfaces. While T_{can} is very sensitive to T_{air} (as expected), it shows almost no sensitivity to thermal properties and latitude; T_{can} is most sensitive to the frontal area ratio λ_f and weakly sensitive to wind speed and Bowen ratio. The wall temperature T_{wall} is less sensitive to λ_f than T_{can}, but more sensitive to the other parameters, especially (in order of sensitivity) wind speed, ground albedo, latitude, building plan area ratio λ_p, and Bowen ratio. As expected, wind speed is anticorrelated with T_{wall}, while ground albedo, Bowen ratio, T_{air}, λ_p, and latitude are positively correlated with T_{wall}. Most notably, an increase in the ground albedo causes a strong increase in wall temperature especially for grass, which supports the argument that a large albedo at ground level may increase heat conduction into buildings. Generally, the T_{wall} sensitivity for grass and AT is comparable, indicating robustness of our results. The direction of the effect or the magnitude of the sensitivity varies between the 20% increases and 20% decreases, suggesting some nonlinearity in the model.

For the soil types specified in our study, the thermal damping depth ranges from 0.10 to 0.14 m, so the soil

TABLE 4. Magnitude and timing of maximum sensible heat fluxes from ground, wall, and roof to canopy air.

	Max ground sensible heat flux (W m^{-2} of ground)	Time (LST)	Max wall sensible heat flux (W m^{-2} of wall)	Time (LST)	Max roof sensible heat flux (W m^{-2} of roof)	Time (LST)
AT	487	1200	132	1400	568	1200
Asphalt	264	1300	154	1400	576	1200
Concrete	211	1300	175	1400	581	1200
Grass	103	1300	133	1400	582	1200

Unauthenticated | Downloaded 03/26/25 07:04 AM UTC

TABLE 5. Cumulative sensible heat fluxes over a day from the urban canopy and roof top to the ABL and the resulting air temperature differences ΔT averaged over a stagnant dry ABL of thickness 2 km.

	Sensible heat flux from canopy to above canopy (kW h m^{-2} of urban area)	ΔT (°C)	Sensible heat flux from roof top to above canopy (kW h m^{-2} of urban area)	ΔT (°C)
Grass	1.11	1.8	0.6	0.98
Concrete	1.93	3.1	0.6	0.98
Asphalt	2.32	3.7	0.6	0.98
AT	3.41	5.5	0.59	0.96

layers below 0.14 m do not contribute significantly to the surface energy budget. At a depth equal to 3 times the damping depth, the range in temperature is 5% of that at the surface (Bonan 2002).

4. Discussion and conclusions

a. Direct temperature and heat flux effects of AT on nearby buildings

The Temperatures of Urban Facets in 3D model was used to compare the impact of different ground surface materials (artificial turf, grass, asphalt, and concrete) on urban canopy layer energy exchange and building energy use. Our comparison covers a clear summer day over a uniform array of buildings at a latitude of 33° with building plan area fraction (λ_p) of 0.15, and frontal area fraction (λ_f) of 0.086.

Comparison of ground surface temperature (Fig. 5a) shows that—as expected—evaporative cooling makes grass by far the coolest surface compared to asphalt, AT, and concrete. This results in larger longwave radiation fluxes (Fig. 8a) from AT—as well as asphalt and concrete—providing substantially more radiative heat to the building walls than grass. However, the total radiative heat transfer from ground to building wall is the sum of reflected solar shortwave and thermal longwave radiation. Since AT has the lowest albedo of the urban surface materials (or almost any surface in the environment, for that matter), AT leads to a substantial reduction in shortwave radiative heat transfer from the ground to the building (Fig. 8b), balancing the increase in longwave radiation. From this point of view the low albedo of AT is a positive characteristic.

The largest sensible heat flux from ground to canopy occurs over AT (Fig. 9). The reasons are high surface temperature (Fig. 5a), lack of water availability (unlike grass), and higher surface roughness (than asphalt and concrete; Table 1). Hence AT increases the canopy air

TABLE 6. Sensitivity of T_{can} and T_{wall} for grass and AT to wind speed, ground properties, λ_p, λ_f, above-canopy air temperature, Bowen ratio, and latitude. The units of the sensitivity are °C per 20% change in the property listed in the first column. Base values for ground properties are presented in Table 1, and for λ_p, λ_f, and latitude are presented in section 2c. The reference values are wind speed of 3 m s^{-1}, maximum T_{air} of 22.67°C, and Bowen ratio of 0.3.

	%	$(T_{can})_{max}$ sensitivity grass	$(T_{wall})_{max}$ sensitivity grass	$(T_{can})_{max}$ sensitivity AT	$(T_{wall})_{max}$ sensitivity AT
Wind speed (m s^{-1})	−20	−0.09	−0.83	−0.11	−0.93
	+20	−0.08	−0.71	−0.12	−0.82
Ground albedo	−20	−0.02	0.54	−0.03	0.11
	+20	−0.03	0.55	−0.04	0.11
Ground thermal conductivity (W m^{-1} K^{-1})	−20	−0.01	−0.01	0.00	−0.01
	+20	−0.01	0.00	0.01	0.05
Ground heat capacity (J m^{-3} K^{-1})	−20	−0.01	−0.01	−0.01	−0.04
	+20	−0.01	−0.01	−0.01	0.00
Building plan area ratio (λ_p)	−20	0.01	0.14	−0.08	0.10
	+20	0.06	0.20	−0.01	0.18
Frontal area ratio (λ_f)	−20	−0.2	0.04	−0.5	−0.22
	+20	−0.05	−0.01	−0.21	−0.03
Latitude	−20	0.00	0.47	−0.03	0.49
	+20	−0.01	0.43	−0.08	0.36
Air temperature (°C)	−20	4.5	4.2	4.5	4.26
	+20	4.49	4.19	4.49	4.24
Bowen ratio	−20	0.08	0.15	—	—
	+20	0.07	0.13	—	—

Unauthenticated | Downloaded 03/26/25 07:04 AM UTC

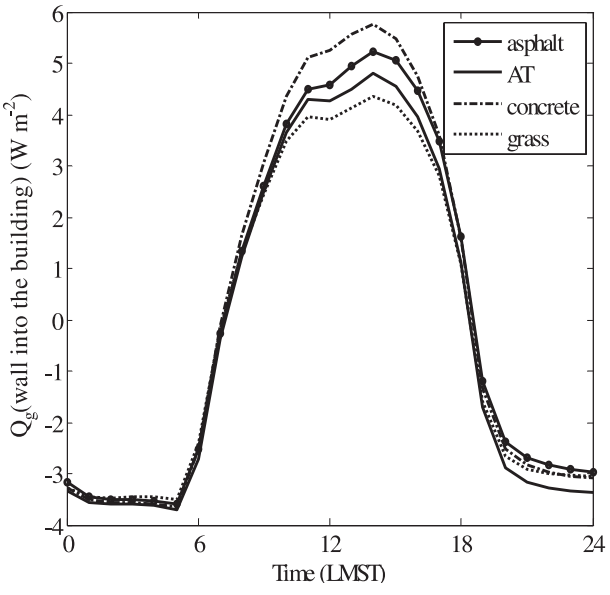

FIG. 10. Comparison of $Q_{g\text{-wall}}$ at the innermost wall layer for AT, grass, asphalt, and concrete; $Q_{g\text{-wall}}$ is averaged over all walls and shown per unit of wall surface area.

temperature (Fig. 5b). The associated decrease in building wall-to-canopy sensible heat fluxes increases building wall temperatures and wall conductive heat fluxes.

b. Implications for building energy use

In this analysis we neglect energy use related to production and disposal of AT, as well as grass maintenance (lawn mowing, fertilizer), which we deem small over the life cycle. Then, the effect of a ground surface material on building energy use will be a function of heat gain or loss due to conduction into the building ($Q_{g\text{-roof}}$ and $Q_{g\text{-wall}}$; Fig. 2), leakage or ventilation of indoor air, and shortwave transmission through windows. With the exception of $Q_{g\text{-wall}}$ and $Q_{g\text{-roof}}$, these processes are not explicitly simulated in TUF3D, so the simulated indoor air temperature (Fig. 4) describes that of an unventilated building without windows. The maximum $Q_{g\text{-wall}}$ at the innermost wall layer for grass is 4.3 W m^{-2} and for AT is 4.8 W m^{-2} (Fig. 10). Thus, relative to grass, AT increases the conductive heat gain through walls by 10%, corresponding to 788 W at peak over the surface area of the building. Note that $Q_{g\text{-wall}}$ is strongly dependent on building envelope parameters, in particular the thermal conductivity, heat capacity, and window fraction. For a given wall net radiation, the relative resistance to heat transfer into the building wall versus convectively into the canopy will determine the ratio of $Q_{g\text{-wall}}$ to canopy sensible heat flux. Thus, our results for $Q_{g\text{-wall}}$ apply mostly to post-1980 construction that follows California Title 24 building standards (Akbari and Konopacki 2005).

TABLE 7. Building heat gain through different physical processes and surfaces according to ASHRAE (Howell et al. 1998) for grass and AT.

Cooling load corresponds to heat gain through	For grass (kW)	For AT (kW)
Roof conduction	1.17	1.27
Wall conduction	2.79	3.22
Glass conduction	−0.70	0.32
Infiltration	0.08	0.55
Nonglass radiation subtotal	3.34	5.36
Glass radiation	38.2	29.4
Total	41.54	34.76

Offline modeling was used to quantify total building energy use using the ''nonresidential cooling load calculation'' method of the American Society of Heating, Refrigerating and Air-Conditioning Engineers (ASHRAE; Howell et al. 1998). In this method the cooling load is the aggregate of conductive heat gain through windows, walls, and roofs; solar heat gain through fenestrations; internal heat gain from lights, people, and equipment; and the heat gain or loss from infiltration and ventilation. We calculated cooling load for AT and grass at a typical summer peak load time at 1400 LST assuming (i) zero internal heat gain, (ii) that 20% of wall surface area is windows exposed to the shortwave radiation calculated through TUF (Fig. 8) and with a solar heat gain coefficient of 0.4 and without blinds, (iii) comfort internal building temperature of 74°F (~23°C) and outdoor air temperature T_{can}, and (iv) no fan energy use (Table 7). The reduction in shortwave radiation through windows (Fig. 8b) resulting from the low AT albedo makes buildings near AT have a 17% lower design cooling load. The significant wall insulation and relatively cool outdoor air in the selected climate zone cause the conduction and ventilation cooling loads to be small compared to the window radiative cooling load. AT does, however, cause a 60% increase in the cooling loads for ventilation and conduction because of the higher canopy air temperature.

Moreover, since water has an embodied energy (i.e., energy that was used in making a product) related to supply, conveyance, treatment, and distribution, the air cooling effects of water come at an (energy) price. For outdoor uses in Southern California, the California Energy Commission (Navigant Consulting 2006) estimated water embodied energy at 11 MW h Mgal^{-1}. Given our evapotranspiration estimate of 3.6 mm day^{-1} per meter squared of grass, and the landscaping area associated with one building of 3867 m^2, we estimate a water use of 13.9 m^3 day^{-1} or 3678 gal day^{-1}. Consequently the

Unauthenticated | Downloaded 03/26/25 07:04 AM UTC

associated energy use would be 40 kW h day^{-1}, which corresponds to a constant power draw of 1.7 kW. This is larger than the online wall heat flux (Fig. 10) and about equal to the offline cooling load penalty of AT during the peak hour (Table 7) if window radiation is ignored, and can be expected to be larger than said penalty over the day. The reduction in water use contributes to the overall local reduction in energy use for AT relative to grass.

AT has nonlocal effects on urban energy use through enhanced canopy layer temperatures, increasing infiltration and ventilation energy use downwind of AT. This nonlocal effect would be largest on days with calm winds as heat would accumulate over the day (Table 5). In moderate winds, the additional heating compared to grass may be as much as 0.11°C km^{-1} that the ABL interacts with an urban area. As they are derived from offline modeling, these results may somewhat overestimate the thermal impacts of AT on the boundary layer. To minimize nonlocal temperature impacts in urban areas with persistent wind directions, AT could be installed preferentially on downwind sides of the urban area. Bornstein et al. (2009) demonstrated that in California, additional inland heating as a result of global warming decreases coastal temperatures, likely through an increase in the sea-breeze intensity. Increased inland (i.e., downwind) installation of AT would presumably strengthen this effect, leading to a more complex mesoscale coupling that is beyond the scope of this study.

The increase in nonlocal energy use caused by AT is estimated using the concept of cooling degree days (CDD; Akbari and Konopacki 2005). The CDD are computed by subtracting 65°F (~18°C) from the average of daily maximum and minimum temperatures (Oliver 2005). We assume that the average grass fraction in California's urban areas is 22% (Walters 2005) and use linear scaling of the results in Table 5 with AT and grass land cover fraction.

From the TMY3 temperatures at Miramar airport weather station and the results in Table 5 for stagnant or recirculating air (the worst case), we determined that replacing all natural grass surfaces with AT would cause an additional 0.6°C CDD. For California, the Department of Energy (DOE) Energy Efficiency and Renewable Energy Web site states that 5.0 kW h in energy are used per capita per CDD (°C). Assuming the typical persons per household in a building (2.87) on a typical summer day, AT would be responsible for (5.0 kW h/person CDD) × 2.87 persons × 0.6 CDD = 8.61 kW h day^{-1} in additional energy use, which is small relative to the values in Table 7. We note that this number would be much larger for warmer locations.

In summary, the net effect of replacement of grass surfaces with AT in coastal Southern California is a net water and energy savings. This is a somewhat unexpected result. While our results appear to be reasonably insensitive to model parameters, more comprehensive analyses of the effects of AT in different building fabrics and climate zones will be necessary to robustly estimate the energy impacts of widespread AT installation. Furthermore, online modeling of the interactions between buildings and their environment throughout the year would potentially yield more accurate results. We also note that other landscaping options such as low–water use plants are available that would significantly reduce water and its embodied energy use compared to grass. Since the albedo of low–water use plants typically is lower than that of grass, we would expect that low–water use plants would have similar effects as AT.

Acknowledgments. We acknowledge funding by the Hellman Foundation and NSF CBET-0847054. Samer Naif assisted with albedo measurements of artificial turf. We thank the University of San Diego and La Costa Canyon High School for allowing access to their athletic fields. Thanks are given to Anthony Dominguez (UCSD) and Ronnen Levinson (Lawrence Berkeley National Lab) for suggesting materials and thermal parameters for California buildings. Three anonymous reviewers helped in substantially improving the manuscript.

REFERENCES

Akbari, H., and S. Konopacki, 2005: Calculating energy-saving potentials of heat-island reduction strategies. *Energy Policy,* **33,** 721–756.

Arnfield, A., 1990: Canyon geometry, the urban fabric and nocturnal cooling: A simulation approach. *Phys. Geogr.,* **11,** 220–239.

Ashdown, I., 1994: *Radiosity: A Programmer's Perspective*. John Wiley & Sons, 496 pp.

Bonan, G. B., 2002: *Ecological Climatology*. Cambridge University Press, 678 pp.

Bornstein, R., 1987: Mean diurnal circulation and thermodynamic evolution of urban boundary layers. *Modelling the Urban Boundary Layer,* Amer. Meteor. Soc., 53–94.

——, B. Lebassi, E. Maurer, P. Switzer, and J. E. Gonzalez, 2009: Cooling summer daytime temperatures in two urban coastal California air basins during 1948–2005: Observations and implications. Preprints, *Eighth Conf. on Coastal Atmospheric and Oceanic Prediction and Processes,* Phoenix, AZ, Amer. Meteor. Soc., J21.1. [Available online at http://ams.confex.com/ams/pdfpapers/146853.pdf.]

Brutsaert, W., 1982: *Evaporation into the Atmosphere*. D. Reidel, 299 pp.

California Climate Zone 7, cited 2009: Title 24 requirements. [Available online at http://www.pge.com/includes/docs/pdfs/about/edusafety/training/pec/toolbox/arch/climate/california_climate_zone_07.pdf.]

Unauthenticated | Downloaded 03/26/25 07:04 AM UTC

Campbell, G. S., and J. M. Norman, 1998: *An Introduction to Environmental Biophysics*. Springer, 286 pp.

Chen, D., T. Gustavsson, and J. Borgen, 1999: The applicability of similarity theory to a road surface. *Meteor. Appl.,* **6,** 81–88.

Dhakal, S., and K. Hanaki, 2002: Improvement of urban thermal environment by managing heat discharge sources and surface modification in Tokyo. *Energy Build.,* **34,** 13–23.

Energy Efficiency and Renewable Energy, cited 2009: Residential consumption of electricity per capita per cooling degree day. [Available online at http://apps1.eere.energy.gov/states/residential.cfm/state=CA#eleccool.]

Galassi, G., and G. Bortolin, cited 2009: New study finds artificial turf may be too hot for summer use. [Available online at http://www.synturf.org/images/UNLV-http___news.dri.edu_nr2008_Artificial_Turf_Research_091808.pdf.]

Giridharan, R., S. Ganesan, and S. Lau, 2004: Daytime urban heat island effect in high-rise and high-density residential developments in Hong Kong. *Energy Build.,* **36,** 525–534.

Grimmond, C. S. B., and T. R. Oke, 2002: Turbulent heat fluxes in urban areas: Observations and a Local-Scale Urban Meteorological Parameterization Scheme (LUMPS). *J. Appl. Meteor.,* **41,** 792–810.

Harman, I., J. Barlow, and S. Belcher, 2004: Scalar fluxes from urban street canyons. Part II: Model. *Bound.-Layer Meteor.,* **113,** 387–409.

Howell, R. H., H. J. Sauer, and W. J. Coad, 1998: *Principles of Heating Ventilating and Air Conditioning*. American Society of Heating, Refrigerating and Air-Conditioning Engineers, 254 pp.

Iqbal, M., 1983: *An Introduction to Solar Radiation*. Academic Press, 390 pp.

Jansson, C., E. Almkvist, and P. Jansson, 2006: Heat balance of an asphalt surface: Observations and physically-based simulations. *Meteor. Appl.,* **13,** 203–221.

Krayenhoff, E. S., 2005: A micro-scale 3-D urban energy balance model for studying surface temperatures. M.S. thesis, Dept. of Geography, University of Western Ontario, 232 pp.

——, and J. A. Voogt, 2004: Sensitivity testing of an urban surface scheme coupled to a 1-D boundary layer model. Preprints, *Fifth Conf. on the Urban Environment,* Vancouver, BC, Canada, Amer. Meteor. Soc., 5.5. [Available online at http://ams.confex.com/ams/pdfpapers/80011.pdf.]

——, and ——, 2007: A microscale three-dimensional urban energy balance model for studying surface temperatures. *Bound.-Layer Meteor.,* **123,** 433–461.

Kruger, E. L., and D. Pearlmutter, 2008: The effect of urban evaporation on building energy demand in an arid environment. *Energy Build.,* **40,** 2090–2098.

Mascart, P., J. Noilhan, and H. Giordani, 1995: A modified parameterization of flux–profile relationships in the surface layer using different roughness length values for heat and momentum. *Bound.-Layer Meteor.,* **72,** 331–344.

Navigant Consulting, 2006: Refining estimates of water-related energy use in California. California Energy Commission Rep. CEC-500-2006-118, 95 pp.

Oke, T. R., 1982: The energetic basis of the urban heat island. *Quart. J. Roy. Meteor. Soc.,* **108,** 1–24.

——, 1987: *Boundary Layer Climates*. Methuen, 435 pp.

——, G. Johnson, D. Steyn, and I. Watson, 1991: Simulation of surface urban heat islands under 'ideal' conditions at night. Part 2: Diagnosis of causation. *Bound.-Layer Meteor.,* **56,** 339–358.

Oliver, J. E., 2005: *Encyclopedia of World Climatology*. Springer, 854 pp.

Speight, J. G., 2005: *Lange's Handbook of Chemistry*. 16th ed. McGraw-Hill, 1572 pp.

Venkatram, A., 2008: Improvement of short-range dispersion models to estimate the air quality impact of power plants in urban environments. California Energy Commission, PIER Energy-Related Environmental Research Program Rep. CEC-500-2007-096, 51 pp.

Walters, A., 2005: Vegetative assessment in an urban environment. California Water Plan Update 2005. [Available online at http://www.waterplan.water.ca.gov/docs/cwpu2005/vol4/vol4-landscapewateruse-vegetativeassessmentinurbanenvironment.pdf.]

Unauthenticated | Downloaded 03/26/25 07:04 AM UTC